CRYSTAL GROWTH & DESIGN

Article

pubs.acs.org/crystal

Azobenzene-Based Organic Salts with Ionic Liquid and Liquid Crystalline Properties

Kathrin Stappert,[†] Johanna Muthmann,[†] Eike T. Spielberg,[†,‡] and Anja-Verena Mudring*[,†,‡,§,∥]

[†]Anorganische Chemie III − Materials Engineering and Characterization, Fakultät für Chemie and Biochemie, Ruhr-Universität Bochum, 44780, Bochum, Germany

[‡]Universitätsbibliothek, Universität Duisburg Essen, Universitätsstrasse 9, 45141 Essen, Germany

[§]Critical Materials Institute, Ames Laboratory, 333 Spedding Hall, Ames, Iowa 50011, United States

[∥]Department of Materials Science and Engineering, Iowa State University, 2220 Hoover Hall, Ames, Iowa 50011, United States

Supporting Information

ABSTRACT: Two sets of new azobenzene-based bromide salts are synthesized, and their thermal photochromic properties are studied. Both sets are based on the imidazolium cation. The first set (**1**) features a symmetric biscation where two imidazolium head groups (Im) with different alkyl chains (Cn) are connected to a central azobenzene unit (Azo): [Azo(C1-Im-Cn)$_2$]; n = 6, 8, 10, 12, 14. The other one contains an *n*-alkyl-imidazolium cation (Cn-Im) bearing a terminal azobenzene unit (C1-Azo) substituted with an alkoxy chain (O-*Cm*) of either two (**2**) or six (**3**) carbon atoms: [C1-Azo-O-*Cm*-Im-Cn]; m = 2, n = 8, 10, 12 and m = 6, n = 8, 10, 12, 14, 16. For both cation classes, the influence of alkyl chains of varying length on the thermal phase behavior was investigated by differential scanning calorimetry (DSC) and polarizing optical microscopy (POM). For five compounds (Azo(-C1-Im-C12)$_2$ (**1d**), Azo(-C1-Im-C12)$_2$ (**1e**), C1-Azo-O-C2-Im-C10 (**2b**), C1-Azo-O-C2-Im-C12 (**2c**), and C1-Azo-O-C6-Im-C16 (**3e**)), the formation of a liquid crystalline phase was observed. The biscationic salts (**1**) are all comparatively high melting organic salts (180−240 °C), and only the two representatives with long alkylchains (C12 and C14) exhibit liquid crystallinity. The monocationic salts with an O−C2 bridge (**2**) melt between 140 and 170 °C depending on the alkyl chain length, but from an alkyl chain of 10 and more carbon atoms on they form a smectic A liquid crystalline phase. The representatives of the third set with a O−C6 bridge qualify as ionic liquids with melting points less than 100 °C. However, only the representative with a hexadecyl chain forms a liquid crystalline phase. Representative single crystals for all sets of cations could be grown that allowed for single crystal structure analysis. Together with small-angle X-ray scattering experiments they allow for a more detailed understanding of the thermal properties. Through irradiation with UV-light (320−366 nm) all compounds undergo *trans*−*cis* isomerization, which reverses under visible light (440 nm).

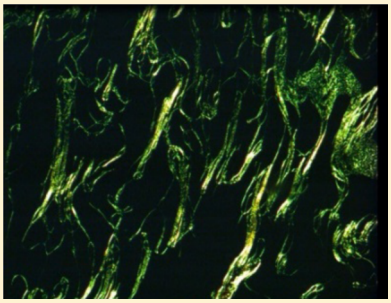

INTRODUCTION

Ionic liquids (ILs) are salts with a melting point below 100 °C.[1] Their unique properties such as low vapor pressure, wide liquid range, good thermal stability, considerable electric conductivity, and large electrochemical window can be tuned by variation of cations and anions.[2] Hence ILs are sometimes called "designer solvents".[3] This makes them very interesting for several applications: among others, they are used as alternative solvents,[4] as electrolytes in dye-sensitized solar cells,[5] and for the electrodeposition of metals[6] but also have been used as a new class of active pharmaceutical ingredient (API).[7] In recent years, a number of cation types for ILs have been developed, but still by far the most commonly used are imidazolium cations. As a consequence, most of the ionic liquid crystals (ILCs) studied so far are based on imidazolium cations. Endowing the imidazolium cation with a long alkyl chain or another mesogenic unit reliably leads to the formation of a mesophase, and these compounds are addressed as ILCs. Thus, ILCs are a subclass of ILs which combine the properties of liquid crystals (LCs) and ILs. As in molecular LCs, the characteristic properties of an ILC depend on the direction in which they are measured and can be influenced by the orientation of the ions. ILCs have been proposed for use in optical, catalytic, electronic, and separation technologies. They can be used as electrolytes with anisotropic conductivity[8] or as "ILC-SILP" (SILP: supported IL phases).[9,10] ILs with calamitic (rod-like) ions usually exhibit lamellar mesophases such as smectic A or smectic C; sometimes also higher ordered phases get stabilized by the electrostatic interactions. Besides calamitic monocationic 1-alkyl-3-methylimidazolium salts[11,12] and related triazolium salts,[13] bicationic imidazolium cations also have been investigated.[14−17] Two types of cation structures that lead to the formation of mesophases can be distinguished:[18] Either the imidazolium cation is endowed with a long alkyl chain and it is itself the mesogenic unit, or the imidazolium acts as the ionic headgroup and is linked to a conventional mesogenic unit.

Received: July 19, 2015
Published: July 23, 2015

DOI: 10.1021/acs.cgd.5b01024
Cryst. Growth Des. 2015, 15, 4701−4712

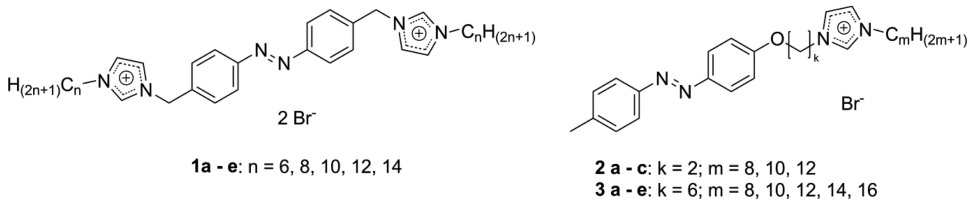

Figure 1. General structure of the synthesized compounds.

Commonly used mesogenic groups are benzyl,[19] biphenyl,[20] or triphenyl[21] or other rigid aromatic systems such as azobenzene[22] with long alkoxy chains.

Azobenzene, with its two phenyl rings separated by an N═N double bond, has attracted considerable attention due to its high optical sensitivity.[23] Upon irradiation with light of appropriate energy (wavelength), it is possible to switch between the two possible isomeric states. In general, the *trans* conformation is thermodynamically preferred and can be converted to the *cis* state by irradiation with UV-light.[24] The reverse transition from the *cis* to the *trans* conformation can either be induced thermally or by visible light. This reversible *cis-trans* photoisomerization process offers a wide range of applications[25] such as optical data storage,[26] optical switching,[27] polarization holography,[28] and the use of azobenzene functionalized molecules as a photolabile surfactants.[29] For this, azobenzene-based polymers and liquid crystalline polymers have been scrutinized intensively.[30] The study of azobenzene based ILCs shows that the ionic character has a great influence on the mesomorphic behavior; for example, as often encountered for ionic LCs, layered, smectic phases are stabilized.[31] In addition to ILCs, ILs with photochromic functionalities have been developed based on the azobenzene,[32] and their photoresponsive conductivity was investigated.[33]

On the basis of these ideas we developed new azobenzene-based salts in order to create novel photoswitchable ILCs. To achieve this, we have chosen a symmetrically imidazolium-substituted bicationic azobenzene system with alkyl chains of various lengths on both sides (**1**) as well as an azobenzene system with just one cationic *n*-alkyl-imidazolium group (**2**, **3**) (Figure 1) where two differently long alkoxy chains are used to connect the azobenzene unit and the imidazolium ring. Bromide was chosen as the counteranion in all cases. The influence of the chain length, symmetry, and crystal structure on the mesophase was investigated with X-ray diffraction (XRD), differential scanning calorimetry (DSC), polarizing optical microscopy (POM), and small-angle X-ray scattering (SAXS). The photochromic properties of all compounds were analyzed with UV−vis spectroscopy.

EXPERIMENTAL SECTION

Synthesis. *Synthesis of 4,4′-Dimethylazobenzene (**5**).* A total of 5.79 g (0.24 mol) of magnesium turnings was washed with water, ethanol, and diethyl ether and then added to a solution of 6.52 g (0.048 mol) of nitrotoluene in 150 mL of methanol. The mixture was stirred at room temperature for 2 h. After addition of water the solution was acidified until just acidic with hydrochloric acid and afterward neutralized with aqueous $NaHCO_3$. The product was purified by column chromatography (cyclohexane/diethyl ether 40:1) and dried overnight at room temperature under a vacuum.

Yield: 2.05 g (9.76 mmol, 40%), ^{1}H NMR (200 MHz, $CDCl_3$) δ: 7.82 (d, J = 8.3 Hz, 4H), 7.31 (d, J = 8.1 Hz, 4H), 2.44 (s, 6H).

*Synthesis of 4,4′-Bis(bromomethyl)azobenzene (**6**).* A mixture of 2.05 g (9.76 mmol) of 4,4′-dimethylazobenzene (**5**), 5.21 g (29.29 mmol) of *N*-bromosuccinimide, and 0.16 g (0.53 mmol) of benzoyl peroxide in chloroform was refluxed for 6 h. After being cooled to room temperature the orange precipitate was filtered off, washed with chloroform and water ,and dried under a vacuum overnight at room temperature.

Yield: 2.42 g (6.58 mmol, 67%), ^{1}H NMR (200 MHz, $CDCl_3$) δ: 7.89 (d, J = 8.5 Hz, 4H), 7.54 (d, J = 8.5 Hz, 4H), 4.56 (s, 4H).

*Synthesis of 4,4′-Bis(N-hexyl imidazole-methyl)azobenzene Dibromide (**1a**).* A total of 0.33 g (0.96 mmol) of compound **6** and 0.59 g (3.86 mmol) of hexyl imidazole were dissolved in acetonitrile and heated under reflux for 20 h. After reaching room temperature the solution was poured onto cold ethyl acetate and stored at −40 °C for several hours. The precipitated orange product was filtered off and dried under a vacuum at room temperature overnight.

Yield: 0.38 g (59%), ^{1}H NMR (200 MHz, DMSO) δ: 9.48 (s, 2H), 7.97−7.85 (m, 8H), 7.66 (d, J = 8.4 Hz, 4H), 5.59 (s,4H), 4.21 (t, J = 7.2 Hz, 4H), 1.84−1.76 (m, 4H), 1.25 (s, 12H), 0.84 (t, J = 6.3 Hz, 6H). ^{13}C NMR (50 MHz, DMSO) δ 151.8, 138.3, 136.3, 129.5, 123.0, 122.9, 122.6, 51.4, 48.9, 40.6, 39.9, 39.7, 39.5−39.3 (m), 39.1, 38.7, 38.3, 30.4, 29.1, 25.1, 21.8, 13.7. MS (FAB): m/z = 153 (32%, hexylimidazole), 208 (98%, 4,4′-dimethylazobenzene$^+$), 256 (100%, K^{+2}/2), 360 (67%, K^{+2}-hexylimidazole), 427 (10%, K^{+2}-C_8H_{17}), 511 (100% K^{+2}-H^+). Elemental analysis: calcd % for $C_{32}H_{44}Br_2N_6$ (M = 672 g/mol): C 57.2, H 6.6, N 12.5 found: C 56.84, H 6.73, N 12.38.

*Synthesis of 4,4′-Bis(N-imidazole-methyl)azobenzene (**9**).* A total of 1.2 g (13.16 mmol) of sodium imidazolide was solved in THF and 2.42 g (6.58 mmol) of compound **6** was added. The mixture was heated under reflux for 20 h and then cooled to room temperature. The excess NaH was filtered off and the solvent was removed under a vacuum. The orange product was dried overnight under vacuum at room temperature.

Yield: 1.62 g (72%), ^{1}H NMR (200 MHz, $CDCl_3$) δ: 7.90 (d, J = 8.2 Hz, 4H), 7.66 (s, 2H), 7.30 (d, J = 8.3 Hz, 4H), 7.14 (s, 2H), 6.95 (s, 2H), 5.22 (s, 4H).

*Synthesis of 4,4′-Bis(N-alkylimidazole-methyl)azobenzene Dibromide (**1b**−**e**).* A solution of compound **9** and 4 equiv of the respective alkyl bromide in acetonitrile was heated under reflux for 6 days, cooled to room temperature, and poured into cold ethyl acetate. The precipitated orange product was dried under a vacuum overnight at room temperature.

*4,4′-Bis(N-octylimidazole-methyl)azobenzene Dibromide (**1b**).* Yield: 52%, ^{1}H NMR (200 MHz, DMSO) δ: 9.36 (s, 2H), 7.97−7.84 (m, 8H), 7.63 (d, J = 8.4 Hz, 4H), 5.55 (s, 4H), 4.19 (t, J = 7.2 Hz, 4H), 1.88−1.70 (m, 4H), 1.23 (s, 20H), 0.84 (t, J = 6.5 Hz, 6H). ^{13}C NMR (50 MHz, MeOD) δ: 153.9, 138.7, 137.5, 130.7, 124.7, 124.2, 123.9, 53.6, 51.1, 32.8, 31.0, 30.2, 29.9, 27.2, 23.6, 14.4. MS (FAB): m/z = 208 (40%, 4,4′-dimethylazobenzene$^+$), 293 (100%, dioctylimidazole$^+$), 388 (30%, K^{+2}-octylimidazole), 455 (12%, K^{+2}-C_8H_{17}), 567 (29% K^{+2}-H^+). Elemental analysis: calcd % for $C_{36}H_{52}Br_2N_6$ (M = 728 g/mol): C 59.3, H 7.2, N 11.5 found: C 57.61, H 7.24, N 11.63.

*4,4′-Bis(N-decylimidazole-methyl)azobenzene Dibromide (**1c**).* Yield: 55%,^{1}H NMR (200 MHz, DMSO) δ: 9.40 (s, 2H), 7.91 (dd, J = 9.5, 5.1 Hz, 8H), 7.64 (d, J = 8.4 Hz, 4H), 5.56 (s, 4H), 4.19 (t, J = 7.1 Hz, 4H), 1.79 (s, 4H), 1.22 (s, 28H), 0.83 (t, J = 6.2 Hz, 6H). ^{13}C NMR (50 MHz, DMSO) δ: 151.8, 138.3, 136.3, 129.4, 123.1, 122.9, 122.7, 51.4, 48.9, 31.2, 29.2, 28.8, 28.6, 28.3, 25.4, 22.0, 13.9. MS (FAB): m/z = 208 (100%, 4,4′-dimethylazobenzene$^+$), 312 (30%, K^{+2}/2), 416 (72%, K^{+2}-decylimidazole), 624 (73% K^{+2}-H^+), 706 (25%, K^{+2}+Br^-).

*4,4′-Bis(N-dodecylimidazole-methyl)azobenzene Dibromide (**1d**).* Yield: 43%, ^{1}H NMR (200 MHz, DMSO) δ: 9.34 (s, 2H), 7.93 (d, J = 8.2 Hz, 4H), 7.85 (s, 4H), 7.62 (d, J = 8.4 Hz, 4H), 5.54 (s, 4H), 4.19 (t, J = 7.0 Hz, 4H), 1.90−1.68 (m, 4H), 1.21 (s, 34H), 0.83 (s, 6H). ^{13}C NMR (50 MHz, DMSO) δ: 151.8, 138.3, 136.3, 129.4, 123.1, 122.9, 122.6,

DOI: 10.1021/acs.cgd.5b01024
Cryst. Growth Des. 2015, 15, 4701−4712

51.4, 49.0, 31.2, 29.2, 28.9, 28.9, 28.8, 28.8, 28.6, 28.3, 25.4, 22.0, 13.9. MS (FAB): m/z = 208 (100%, 4,4′-dimethylazobenzene^{+}), 340 (15%, K^{+2}/2), 444 (50%, K^{+2}-dodecylimidazole), 679 (54% K^{+2}-H^{+}), 761 (15%, K^{+2}+Br^{-}). Elemental analysis: calcd % for $C_{44}H_{68}Br_2N_6$ (M = 840 g/mol): C 62.85, H 8.15, N 9.99 found: C 58.26, H 7.97, N 9.98.

*4,4′-Bis(N-tetradecylimidazole-methyl)azobenzene Dibromide (**1e**).* Yield: 40%, ^{1}H NMR (200 MHz, DMSO) δ 9.33 (s, 2H), 7.92 (d, J = 8.3 Hz, 4H), 7.85 (s, 2H), 7.62 (d, J = 8.6 Hz, 4H), 5.54 (s, 4H), 4.19 (t, J = 6.8 Hz, 4H), 1.86−1.70 (m, 4H), 1.21 (s, 45H), 0.84 (t, J = 3.3 Hz, 6H). ^{13}C NMR (50 MHz, DMSO) δ: 151.8, 138.3, 136.3, 129.4, 123.1, 122.9, 122.7, 51.5, 49.0, 35.8, 31.2, 29.2, 28.9, 28.9, 28.8, 28.8, 28.6, 28.3, 25.4, 22.0, 13.9. MS (FAB): m/z = 208 (83%, 4,4′-dimethylazobenzene^{+}), 368 (37%, K^{+2}/2), 461 (100%, ditetradecylimidazolium), 472 (79%, K^{+2}-tetradecylimidazole), 539 (19%, K^{+2}-$C_{14}H_{29}$), 735 (69% K^{+2}-H^{+}), 817 (23%, K^{+2}+Br^{-}). Elemental analysis: calcd % for $C_{48}H_{76}Br_2N_6$ (M = 897 g/mol): C 64.3, H 8.5, N 9.4 found: C 60.1, H 8.15, N 9.73.

*Synthesis of 4-Methylphenyldiazenylphenol **13**.* Ten grams of p-toluidine (93.45 mmol) and 25 mL of concentrated hydrochloric acid were dissolved in 111 mL of water and cooled to 0 °C. A total of 6.45 g of $NaNO_2$ (93.45 mmol) in 15 mL of water were added slowly. A solution of phenol (8.77g, 93.45 mmol), Na_2CO_3 (10.18 g, 96 mmol), and NaOH (3.84 g, 96 mmol) was added dropwise, and the mixture was stirred for another 4 h. After the pH was adjusted to 7 with hydrochloric acid, the precipitated product was filtered off, washed with water, and dried under a vacuum at room temperature for 24 h.

Yield: 11.9 g (60%), ^{1}H NMR (200 MHz, acetone) δ: 7.88−7.70 (m, 4H), 7.35 (d, J = 8.0 Hz, 2H), 7.06−6.95 (m, 2H), 2.41 (s, 3H).

*Synthesis of 1-(4-((2-Bromoethyl)oxy)phenyl)-2-(4-methylphenyl)diazene **15a**.* A mixture of 3 g (14.15 mmol) of **13**, 3.64 mL (42.45 mmol) of 1,2-dibromoethane, and 7.22 g (52.36 mmol) of K_2CO_3 in 100 mL of acetonitrile was heated under reflux for 20 h. After being cooled to room temperature the suspension was poured into water and extracted with dichloromethane. The combined organic phases were dried with sodium sulfate and filtered, and the solvent was removed under a vacuum. The product was dried under a vacuum at room temperature for 20 h to give an orange powder.

Yield: 1,7 g (38%), ^{1}H NMR (200 MHz, $CDCl_3$) δ: 7.96−7.86 (m, 2H), 7.84−7.74 (m, 2H), 7.30 (d, J = 8.0 Hz, 2H), 7.07−6.97 (m, 2H), 4.38 (t, J = 6.3 Hz, 2H), 3.68 (t, J = 6.3 Hz, 2H), 2.43 (s, 3H).

*Synthesis of 1-Alkyl-(2-(4-((4-methylphenyl)diazenyl)phenoxy)-ethyl)imidazolium Bromide **2 a**−**c**.* A solution of **15a** and 1 equiv of the respective alkylimidazolide was heated under reflux in acetonitrile for 3 days. After being cooled to room temperature the solution was poured into cold ethyl acetate and kept at −40 °C for 12 h. The orange precipitate was filtered off and dried under a vacuum at room temperature overnight.

*1-Octyl-8-(2-(4-((4-methylphenyl)diazenyl)phenoxy)ethyl)-imidazolium Bromide **2a**.* Yield: 54%, ^{1}H NMR (200 MHz, $CDCl_3$) δ: 10.59 (s, 2H), 7.75 (dd, J = 19.1, 8.6 Hz, 4H), 7.58 (s, 1H), 7.22 (d, J = 7.3 Hz, 2H), 7.19 (s, 1H), 6.94 (d, J = 9.0 Hz, 2H), 5.02−4.88 (m, 2H), 4.52−4.39 (m, 2H), 4.28−4.12 (m, 2H), 2.35 (s, 3H), 1.83 (d, J = 6.7 Hz, 2H), 1.29−1.11 (m, 10H), 0.78 (t, J = 5.8 Hz, 3H). ^{13}C NMR (50 MHz, $CDCl_3$) δ: 159.6, 150.7, 147.7, 141.3, 137.4, 129.8, 124.7, 123.5, 122.7, 121.5, 114.8, 66.7, 50.4, 49.5, 31.7, 30.3, 29.1, 28.9, 26.3, 22.6, 21.5, 14.1. MS (FAB): m/z = 419 (100%, K^{+}). Elemental analysis: calcd % for $C_{26}H_{35}BrN_4O$ (M = 499 g/mol): C 62.52, H 7.06, N 11.22 found: C 62.27, H 7.34, N 11.35.

*1-Decyl-10-(2-(4-((4-methylphenyl)diazenyl)phenoxy)ethyl)-imidazolium Bromide **2b**.* Yield: 49%,^{1}H NMR (200 MHz, $CDCl_3$) δ: 10.99 (s, 1H), 7.88 (d, J = 8.9 Hz, 2H), 7.78 (d, J = 8.3 Hz, 2H), 7.55 (s, 1H), 7.31 (s, 2H), 7.18 (s, 1H), 6.99 (d, J = 9.0 Hz, 2H), 5.03 (d, J = 4.7 Hz, 2H), 4.53 (d, J = 4.5 Hz, 2H), 4.30−4.17 (m, 2H), 2.42 (s, 3H), 2.03−1.82 (m, 2H), 1.42−1.14 (m, 18H), 0.86 (t, J = 6.4 Hz, 3H). ^{13}C NMR (50 MHz, $CDCl_3$) δ: 159.6, 150.8, 147.9, 141.4, 138.3, 129.9, 124.8, 123.5, 122.8, 121.0, 114.8, 67.0, 49.6, 31.9, 30.3, 29.5, 29.3, 29.1, 26.4, 22.8, 21.6, 14.2. MS (FAB): m/z = 349 (100%, Didecylimidazol^{+}), 447 (97% K^{+}). Elemental analysis: calcd % for $C_{28}H_{39}BrN_4O$ (M = 527 g/mol): C 63.75, H 7.45, N 10.62 found: C 65.03, H 8.75, N 10.71.

*1-Dodecyl-12-(2-(4-((4-methylphenyl)diazenyl)phenoxy)ethyl)-imidazolium Bromide **2c**.* Yield: 63%, ^{1}H NMR (200 MHz, $CDCl_3$) δ: 10.88 (s, 1H), 7.88 (d, J = 9.0 Hz, 2H), 7.78 (d, J = 8.3 Hz, 2H), 7.55 (s, 1H), 7.29 (d, J = 8.6 Hz, 2H), 7.20−7.14 (m, 1H), 7.00 (d, J = 9.0 Hz, 2H), 5.07−4.98 (m, 2H), 4.58−4.48 (m, 2H), 4.25 (t, J = 7.5 Hz, 2H), 2.42 (s, 3H), 1.91 (d, J = 6.5 Hz, 2H), 1.36−1.19 (m, 18H), 0.87 (t, J = 6.4 Hz, 3H). ^{13}C NMR (50 MHz, $CDCl_3$) δ: 159.6, 150.7, 147.7, 141.3, 137.4, 129.8, 124.7, 123.5, 122.7, 121.5, 114.8, 66.7, 50.4, 49.5, 31.9, 30.3, 29.6, 29.6, 29.4, 29.4, 29.0, 26.3, 22.7, 21.5, 14.2. MS (FAB): m/z = 405 (60%, Didodecylimidazol^{+}), 475 (100% K^{+}). Elemental analysis: calcd % for $C_{30}H_{43}BrN_4O$ (M = 555 g/mol): C 64.85, H 7.80, N 10.08 found: C 65.1, H 8.06, N 9.95.

*Synthesis of 1-(4-((6-Bromohexyl)oxy)phenyl)-2-(4-methylphenyl)diazene **15b**.* This compound was synthesized by the same procedure described for the synthesis of **15a**. From 14-methylphenyldiazenylphenol (**13**) (3 g, 14.15 mmol), dibromohexane (10.36 g, 42.45 mmol) and 7.22 g of potassium carbonate, **15b** was obtained as an orange solid.

^{1}H NMR (200 MHz, acetone) δ: 7.82−7.72 (m, 2H), 7.66 (d, J = 8.3 Hz, 2H), 7.23 (d, J = 8.1 Hz, 2H), 7.03−6.93 (m, 2H), 4.00 (t, J = 6.4 Hz, 2H), 3.40 (t, J = 6.7 Hz, 2H), 2.29 (s, 3H), 1.79−1.71 (m, 6H), 1.64−1.57 (m, 2H), 1.42 (dd, J = 9.0, 5.5 Hz, 4H).

*Synthesis of 1-Alkyl-(2-(4-((4-methylphenyl)diazenyl)phenoxy)-hexyl)imidazolium Bromide **3a**−**e**.* This compound was synthesized by the same procedure described for the synthesis of **2a**−**c**. A solution of **15b** and 1 equiv of the respective alkylimidazole was heated under reflux in acetonitrile for 3 days. After being cooled to room temperature the solution was poured into cold ethyl acetate and kept at −40 °C for 12 h. The orange precipitate was filtered off and dried under a vacuum at room temperature overnight.

*1-Octyl-8-(2-(4-((4-methylphenyl)diazenyl)phenoxy)hexyl)-imidazolium Bromide **3a**.* Yield: 70%, ^{1}H NMR (200 MHz, $CDCl_3$) δ: 10.76 (s, 1H), 7.76 (dd, J = 20.0, 8.6 Hz, 4H), 7.24 (s, 2H), 7.16−7.11 (m, 1H), 6.91 (d, J = 8.9 Hz, 2H), 4.40−4.18 (m, 4H), 3.97 (t, J = 6.1 Hz, 2H), 2.35 (s, 3H), 1.85 (ddd, J = 24.4, 10.8, 5.3 Hz, 6H), 1.56−1.33 (m, 4H), 1.29−1.13 (m, 10H), 0.80 (t, J = 6.2 Hz, 3H). ^{13}C NMR (50 MHz, $CDCl_3$) δ: 161.4, 150.9, 147.0, 140.9, 137.7, 129.8, 124.7, 122.6, 121.8, 121.7, 114.8, 67.9, 50.3, 50.1, 31.8, 30.4, 29.1, 29.0, 28.9, 26.4, 25.9, 25.6, 22.7, 21.6, 14.2. MS (FAB): m/z = 475 (100%, K^{+}), 1031 (2% 2*K^{+}+Br^{-}). Elemental analysis: calcd % for $C_{30}H_{43}BrN_4O$ (M = 555 g/mol): C 64.85, H 7.80, N 10.08 found: C 63.51, H 8.13, N 9.79.

*1-Decyl-10-(2-(4-((4-methylphenyl)diazenyl)phenoxy)hexyl)-imidazolium Bromide **3b**.* Yield: 51%, ^{1}H NMR (200 MHz, $CDCl_3$) δ: 10.81 (s, 1H), 7.82 (dd, J = 19.9, 8.6 Hz, 4H), 7.29 (d, J = 5.5 Hz, 2H), 7.23−7.19 (m, 1H), 6.97 (d, J = 8.9 Hz, 2H), 4.35 (dt, J = 17.9, 7.5 Hz, 4H), 4.03 (t, J = 6.1 Hz, 2H), 2.41 (s, 3H), 1.97−1.77 (m, 6H), 1.47 (d, J = 10.7 Hz, 4H), 1.34−1.20 (m, 14H), 0.86 (t, J = 6.4 Hz, 3H). ^{13}C NMR (50 MHz, $CDCl_3$) δ: 161.4, 150.9, 147.0, 140.9, 137.9, 129.8, 124.7, 122.6, 121.7, 121.6, 114.8, 67.9, 50.3, 50.1, 31.9, 30.4, 29.6, 29.5, 29.4, 29.1, 28.9, 26.4, 26.0, 25.6, 22.8, 21.6, 14.2. MS (FAB): m/z = 503 (100%, K^{+}), 1087 (1.2%, 2*K^{+}+Br^{-}). Elemental analysis: calcd % for $C_{32}H_{47}BrN_4O$ (M = 583 g/mol): C 65.85, H 8.12, N 9.60 found: C 63.9, H 8.14, N 9.23.

*1-Dodecyl-12-(2-(4-((4-methylphenyl)diazenyl)phenoxy)hexyl)-imidazolium Bromide **3c**.* Yield: 66%, ^{1}H NMR (200 MHz, Acetone) δ: 10.29 (s, 1H), 7.94−7.73 (m, 6H), 7.36 (d, J = 8.1 Hz, 2H), 7.11 (d, J = 9.1 Hz, 2H), 4.45 (dt, J = 11.3, 7.3 Hz, 4H), 4.13 (t, J = 6.4 Hz, 2H), 2.42 (s, 3H), 1.82 (dd, J = 16.9, 9.2 Hz, 6H), 1.61−1.43 (m, 4H), 1.30 (d, J = 17.1 Hz, 18H), 0.86 (t, J = 6.4 Hz, 3H). ^{13}C NMR (50 MHz, $CDCl_3$) δ: 161.4, 150.8, 146.9, 140.9, 137.6, 129.8, 124.7, 122.6, 121.9, 121.7, 114.8, 67.9, 50.3, 50.0, 31.9, 30.4, 30.3, 29.7, 29.6, 29.5, 29.4, 29.1, 28.9, 26.4, 25.9, 25.5, 22.8, 21.6, 14.2. MS (FAB): m/z = 531 (100%, K^{+}), 1143 (1.7%, 2*K^{+}+Br^{-}). Elemental analysis: calcd % for $C_{34}H_{51}BrN_4O$ (M = 611 g/mol): C 66.76, H 8.4, N 9.16 found: C 66.54, H 9.44, N 9.07.

*1-Tetradecyl-12-(2-(4-((4-methylphenyl)diazenyl)phenoxy)hexyl)-imidazolium Bromide **3d**.* Yield: 48%, ^{1}H NMR (200 MHz, CD_3CN) δ: 8.68 (s, 1H), 8.04−7.81 (m, 4H), 7.49 (dd, J = 6.0, 4.8 Hz, 4H), 7.16 (dt, J = 4.3, 3.1 Hz, 2H), 4.33−4.10 (m, 6H), 2.53 (s, 3H), 1.91−1.81 (m, 6H), 1.75−1.56 (m, 4H), 1.36 (s, 22H), 0.98 (t, J = 6.5 Hz, 3H). ^{13}C NMR (50 MHz, $CDCl_3$) δ: 161.5, 150.8, 146.9, 141.0, 137.8, 129.8,

DOI: 10.1021/acs.cgd.5b01024
Cryst. Growth Des. 2015, 15, 4701−4712

Scheme 1. Synthesis of Compound 1a−e[a]

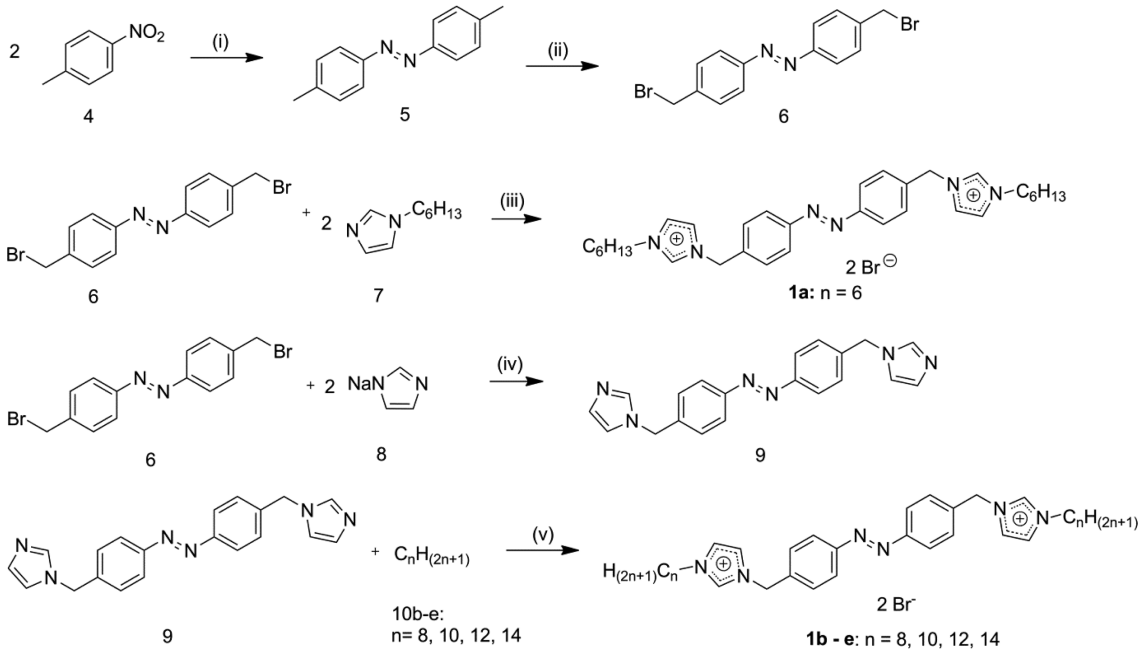

[a](i) MeOH, Mg, rt; (ii) NBS, BPO, $CHCl_3$, reflux, 6 h; (iii) CH_3CN, reflux, 20 h; (iv) THF, reflux, 20 h; (v) CH_3CN, reflux, 20 h.

124.8, 122.6, 121.8, 121.6, 114.8, 67.9, 50.3, 50.1, 32.0, 30.4, 29.8, 29.7, 29.6, 29.5, 29.1, 28.9, 26.4, 26.0, 25.6, 22.8, 21.6, 14.2, 7.9. MS (FAB): m/z = 461 (100%, ditetradecylimidazol$^+$), 559 (42%, K$^+$). Elemental analysis: calcd % for $C_{36}H_{55}BrN_4O$ (M = 639 g/mol): C 67.59, H 8.67, N 8.76 found: C 67.06, H 8.57, N 8.58.

1-Hexadecyl-12-(2-(4-((4-methylphenyl)diazenyl)phenoxy)hexyl)-imidazolium Bromide ***3e***. Yield: 60%, ^{1}H NMR (200 MHz, $CDCl_3$) δ: 10.81 (s, 1H), 7.82 (dd, J = 20.0, 8.5 Hz, 4H), 7.30 (s, 2H), 7.26−7.17 (m, 2H), 6.97 (d, J = 9.0 Hz, 2H), 4.35 (dt, J = 18.5, 7.3 Hz, 4H), 4.03 (t, J = 6.1 Hz, 2H), 2.41 (s, 3H), 2.08−1.74 (m, 6H), 1.50 (s, 4H), 1.26 (d, J = 11.8 Hz, 24H), 0.86 (t, J = 6.4 Hz, 3H). ^{13}C NMR (50 MHz, $CDCl_3$) δ: 161.4, 150.9, 147.1, 140.9, 138.0, 129.8, 124.7, 122.7, 121.6, 121.5, 114.8, 67.9, 50.1, 32.1, 30.4, 29.8, 29.6, 29.5, 29.1, 28.9, 26.4, 26.0, 25.6, 22.8, 21.6, 14.3. MS (FAB): m/z = 517 (100%, dihexadecylimidazol$^+$), 587 (20%, K$^+$). Elemental analysis: calcd % for $C_{38}H_{59}BrN_4O$ (M = 667 g/mol): C 68.34, H 8.91, N 8.39 found: C 67.28, H 8.55, N 8.39.

INSTRUMENTATION

Differential scanning calorimetry (DSC) was performed with a computer-controlled PhoenixDSC 204 F1 thermal analyzer (Netzsch, Selb, Germany). Measurements were carried out at a heating rate of 5 °C/min in sealed aluminum crucible with an argon flow rate of 20 mL/min. The samples were placed in aluminum pans which were cold-sealed. Given temperatures correspond to the onset of the respective thermal process.

Optical analyses were made by heated-stage polarized optical microscopy (POM) with an Axio Imager A1 microscope (Carl Zeiss MicroImaging GmbH,Göttingen, D) equipped with a hot stage, THMS600 (Linkam ScientificInstruments Ltd., Surrey, UK), and Linkam TMS 94 temperature controller (Linkam Scientific Instruments Ltd., Surrey, UK). Images were recorded at a magnification of 100× as a video with a digital camera during heating and cooling the sample which was places between two coverslips. Heating and cooling rates were 5 K/min^{-1}.

Temperature-dependent SAXS experiments were carried out at the BW4 Beamline of DORIS III, Hasylab (DESY, Hamburg, Germany) at a fixed wavelength of 1.38 Å. The data were collected with a MarCCD detector. The detector was calibrated with silver behenate and the sample−detector position was fixed at 455 mm. For measurements, the samples were placed between aluminum foil in a copper sample holder, the sample chamber was evacuated, and the temperature was controlled via a JUMO IMAGO 500 multichannel process and program controller. The program "a2tool" (Hasylab) was used for data reduction, analysis, and correction.

UV−visible absorption spectra were measured at room temperature on solutions in 1 cm cuvettes using an Agilent Cary 50 spectrometer. Photoisomerization experiments were performed in the sample chamber of a Horiba Jobin Yvon Fluorolog-3 spectrometer using the instrument's continuous xenon lamp (450 W) and double grating to achieve monochromatic light. Absorption spectra were recorded within the sample chamber using fiber optics coupled to the Agilent Cary 50 spectrometer via the fiber optic accessory. During all measurements the samples were well stirred and the temperature controlled.

Single crystal X-ray measurements were carried out on a Stoe IPDS-I single-crystal X-ray diffractometer with graphite monochromated Mo Kα radiation (λ = 0.71073 Å at 100 K). Crystal structure solution by direct methods using SIR 92[34] yielded the heavy atom positions. Refinement with SHELXL-97[35] allowed for the localization of the remaining atom positions. Hydrogen atoms were added and treated with the riding atom mode. Data reduction was performed with the program package X-Red[36] and numerical absorption correction was carried out with the program X-Shape.[37] To illustrate the crystal structures, the program Diamond[38] was used.

RESULTS AND DISCUSSION

Synthesis. Two different synthetic routes were chosen for the symmetric (**1**) and the asymmetric azo-compounds (**2** and **3**), both starting with an azobenzene coupling. The first step in the synthesis of the symmetric type **1** cations was the reductive coupling of *p*-nitrotoluene with magnesium (Scheme 1).

DOI: 10.1021/acs.cgd.5b01024
Cryst. Growth Des. 2015, 15, 4701−4712

Scheme 2. Synthesis of Compounds 2a−c and 3a−e[a]

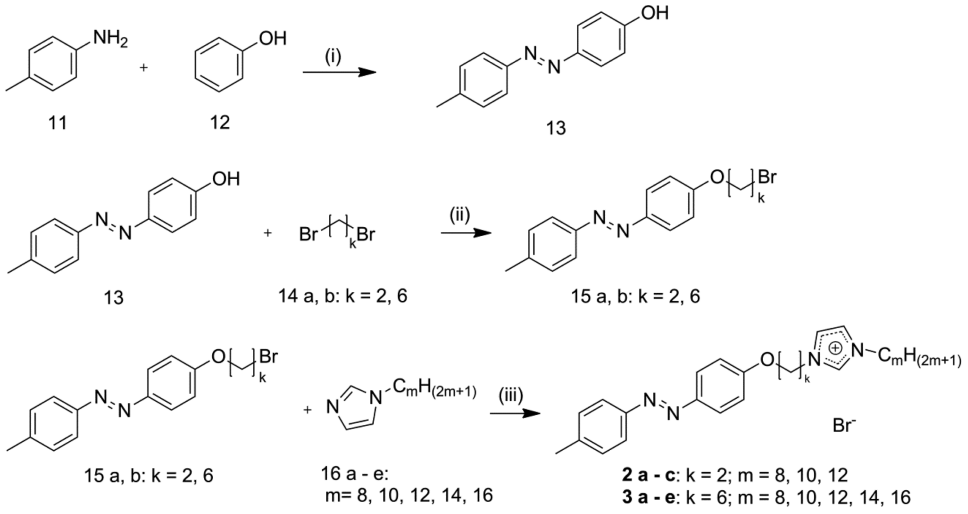

[a](i) $NaNO_2$, NaOH, Na_2CO_3, HCl, H_2O, rt, 4 h; (ii) K_2CO_3, CH_3CN, reflux, 18 h.

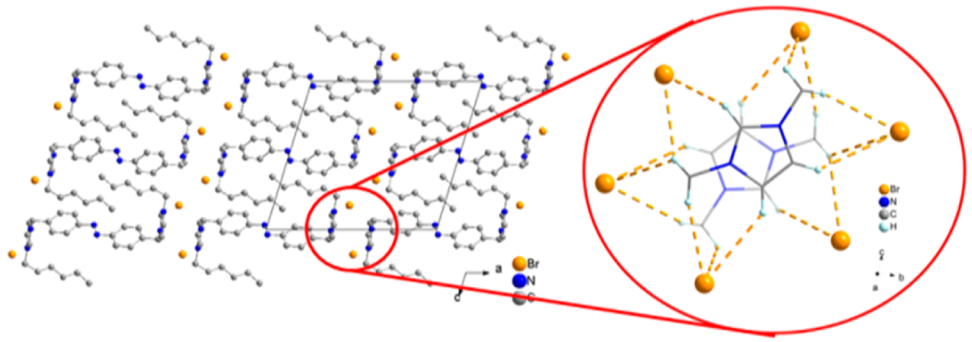

Figure 2. Crystal structure of compound **1a**.

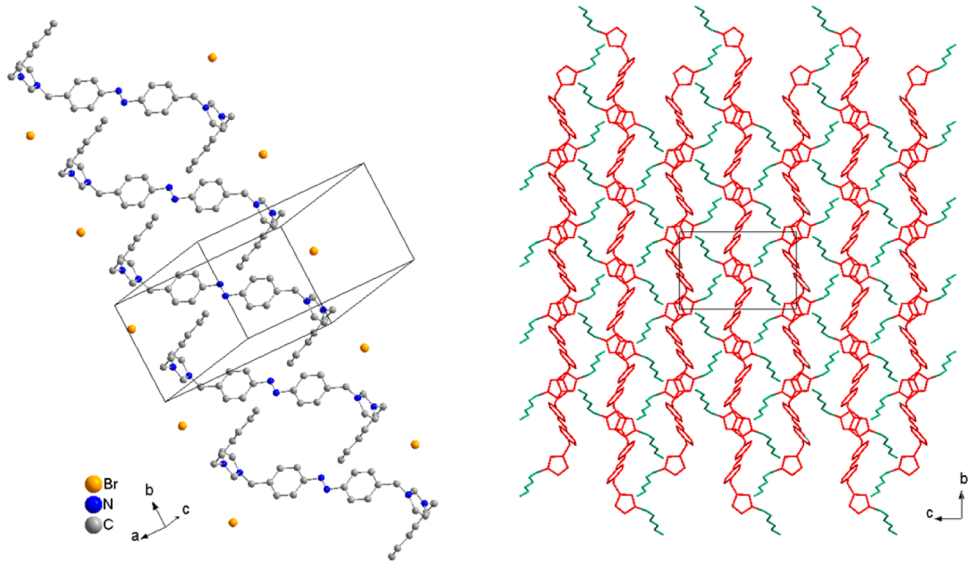

Figure 3. Crystal packing of compound **1a** (left) S-conformation of the cation; (right) structural segregation of polar (red) and apolar (green) domains.

Bromination of the two methyl groups was achieved with bromosuccinimide (NBS) in the presence of benzoyl peroxide (BPO). Addition of hexyl-imidazole results in the formation of the ionic compound **1a**. For the salts with longer alkyl chains the 4,4′-bis(bromomethyl)azobenzene was reacted with sodium imidazolide and then alkylated with the respective alkyl bromide (**1b−e**).

The azobenzene core for the asymmetric compounds was formed via base catalyzed azo-coupling of *p*-methylaniline and phenol (Scheme 2). After formation of the bromo-alkyl-ether the

DOI: 10.1021/acs.cgd.5b01024
Cryst. Growth Des. 2015, 15, 4701−4712

corresponding alkyl-imidazole was alkylated with this to form the compounds **2a−c** and **3a−e**.

Structural Analysis. Representative single crystals for all sets of cations could be grown that allowed for single crystal structure analysis. Single crystals of compound **1a** (Azo(-C1-Im-C6)$_2$) could be grown from methanol solution. **1a** crystallizes in the monoclinic space group $P2_1/c$. The planar azobenzene unit adopts a *trans* conformation, and the imidazolium rings point in opposite directions from the azobenzene with an angle of 107° between the azobenzene plane and a plane through the imidazolium ring (Figure 2). The alkyl chains form an angle of 112° with the imidazolium plane and point back in the direction of the azobenzene unit (Figure 2, left). Thus, a single cation adopts an S-shape configuration with all moieties (azobenzene, imidazole, alkyl chains) in one plane. The two counter bromide anions are located at the top and at the bottom of the S (Figure 3, left) featuring very weak Br···H-interactions (Figure 2, right). Within the *bc*-plane the bications arrange in layers with interdigitated alkyl chains (Figure 2, left). The azobenzene-planes of neighboring cations are perpendicular to each other; thus, the two alkyl chains of one cation interdigitate with those of two other cations.

A structural segregation of polar (red) and apolar (green) domains can be made out within the layers (Figure 3, right). The polar region is composed of aromatic azobenzene units and cationic imidazolium groups. The hydrophobic alkyl chains form the apolar domains. The aromatic parts of different cations form chains through the layer supported by interionic interactions (Figure 3, right). While no $\pi-\pi$ interactions can be detected for the azobenzene units, $\pi-\pi$ interactions can be assumed between the imidazolium rings, although positively charged, as the distance between imidazolium cations belonging to two different layers is rather small (3.5 Å).

Single crystals of compounds **2a−c** could be grown either from a dichloromethane solution or a mixture of dichloromethane and acetonitrile. Compound **2a** (C1-Azo-O-C2-Im-C8) crystallizes in the acentric triclinic space group $P1$, compound **2b** (C1-Azo-O-C2-Im-C10), and **2c** (C1-Azo-O-C2-Im-C12) crystallize in the triclinic space group $P\bar{1}$. The azobenzene unit adopts the generally thermodynamically favored *trans* conformation in all three structures. In **2a** the imidazolium ring is situated perpendicular to the planar azobenzene group as well as to the alkyl chain which is parallel to the azobenzene leading to an U-shape of the cation (Figure 6, left). The bromide anions in **2a** are involved in hydrogen bonding with the first carbon-H of the chain (Figure 4, Table 1), whereas in **2b** and **2c** one of the two CH-groups of the triazolium ring forms C−H···Br hydrogen bonds to the bromide anion (Figure 5).

The crystal structure of **2a** shows that the cations form a bilayer structure with head-to-head arranged triazolium groups alternating with bromide counteranions. Within the bilayer the opposing cations are tilted with an angle of about 60° (Figure 6, left).

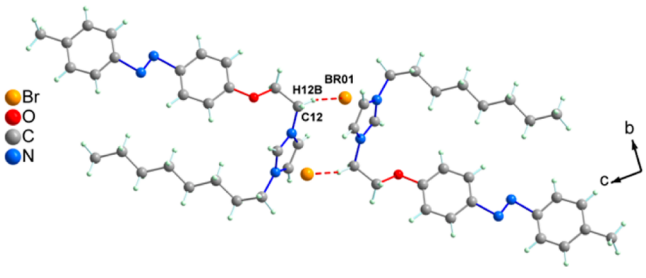

Figure 4. Hydrogen bonding interactions in detail for **2a**.

In **2b** the cations also adopt a U-shape, but single layers are formed by head-to-tail arranged cationic entities (Figure 6, right). Thus, within one layer (parallel to the *a*,*c* plane), all cations have the same orientation. Along the *b*-axis the orientation of the cations alternates, and the open sides of the "U" are facing in opposite directions.

The crystal structure of **2c** is distinctly different to the other two structures, because the two sides of the "U" units are forced apart and the ion is rather resembling a L (Figure 7, right). Viewed along the *a*-axis the alkyl chain and the azobenzene unit are perpendicular to the imidazolium ring and parallel to each other (Figure 7, left). The cations make up a bilayer with a head-to-head arrangement of the imidazolium cores. When viewed along the *b*-axis, it becomes obvious that the cations no longer resemble a U but more an L (Figure 7, right). The angle between the arms of one cation is about 90°. (Measured as the angle between the first carbon of the alkyl chain, the C2 of the imidazolium ring and the methyl group at the *para* position of the azobenzene.) Layers with alternating charged, polar and apolar domains are visible in all three structures (**2a**, **2b**, and **2c**). The compounds with the shortest (C_8H_{17}) and with the longest ($C_{12}H_{25}$) alkyl chain feature bilayers with head-to-head arranged cations. In contrast, the salt with an intermediate chain length of 10 carbon atoms (**2b**) forms a single layered structure. From the imidazolium ring to the methyl group of the azobenzene a distance of about 14 Å is measured in all three crystal structures. The $C_{12}H_{25}$ chain has approximately the same length as this entity, while being shorter for **2b** (11.5 Å) and **2a** (8.9 Å), respectively. Thus, with varying the alkyl chain length the relative influence of the different interactions ($\pi-\pi$ vs van-der-Waals vs ionic) is shifted, and as a consequence, the ion packing and the crystal structure changes.

The compounds **3c** and **3e** crystallize in the monoclinic space group $P2_1/c$ and are isostructural; therefore only the crystal structure of compound **3e** will be discussed here in detail. As expected, the planar azobenzene unit has a *trans* conformation. The two alkyl chains stretch out in opposite directions from the imidazolium head (Figure 8). The terminal hexadecyl chain has an *all trans* conformation except for the bond from the carbon atom connected to the imidazolium core and the second carbon of the alkyl chain. The middle hexyl chain starts in *trans* conformation from the imidazolium but is bent in the middle. The bonds from the fourth to the fifth and from the fifth to the sixth carbon atom in this row are *gauche*. Thus, the cations adopt a zigzag structure with parallel arrangement (Figure 9). Within the layers two cations form a pair and cross each other in the middle (Figure 8). The orientation of these ion pairs is alternating from layer to layer, so that always the alkyl tail of one cation is facing the azobenzene unit of the cation in the next layer. The cationic imidazolium head lies in the middle of the layers surrounded by the bromide counteranions.

Thermal Behavior. The thermal properties of all compounds were examined by POM and DSC. The transition temperatures, enthalpies, and phase transition assignments are listed in Table 2. Discrepancies to various degrees both in the transition temperatures as well as enthalpies between heating and cooling cycles are observed. The reason for this lies in the slow transition kinetics which prevent that thermodynamic equilibrium is reached. Thus, supercooling and incomplete phase

DOI: 10.1021/acs.cgd.5b01024
Cryst. Growth Des. 2015, 15, 4701−4712

Table 1. Hydrogen Bond Details for 2a, 2b, and 2c

	C1-Azo-O-C2-Im-C8	C1-Azo-O-C2-Im-C10	C1-Azo-O-C2-Im-C12
	C12−H12B···Br	C17−H17···Br	C13−H13···Br
H···A (Å)	2.9457(6)	2.6544(4)	2.8247(3)
H···A (deg)	150.328(2)	170.863(2)	160.496(1)

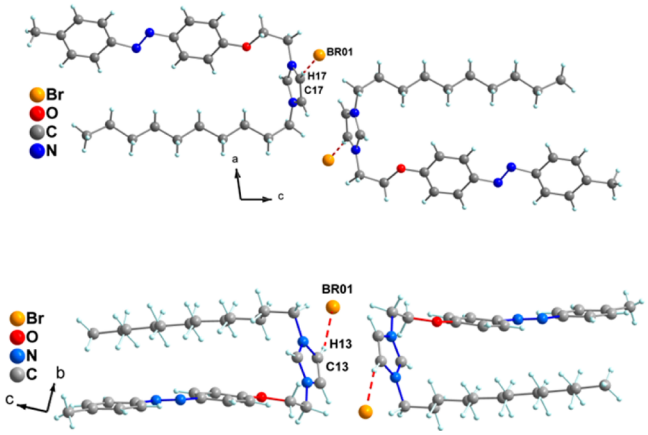

Figure 5. Hydrogen bonding interactions in detail for **2b** (top) and **2c** (bottom).

transitions are favored, a phenomenon quite often observed for compounds that belong to the class of ILs.

Figure 10 shows the heating curves of the symmetric azobenzene salts **1a**−**e**. For all five compounds decomposition begins when the substances are about to melt. Therefore, the cooling curves are featureless (not shown here). **1a** and **1b** with the shortest alkyl chains melt into an isotropic liquid at 212 and 225 °C without showing signs for a preceding phase transitions. **1c** melts in the same temperature region (222 °C) but features an additional thermal effect around 140 °C. As no phase change could be observed by POM, we attribute this thermal event to a solid−solid phase transition. For the salts with the longer alkyl chains the melting points and decomposition temperatures are slightly lower. **1d** exhibits the formation of a mesophase around 150 °C and **1e** around 100 °C. The thermal event at lower temperature (75 °C) is due to a solid−solid phase transition.

Figure 11 shows the second heating cycle of the asymmetric azobenzene compounds with the short alkyl chains in the middle (**2a**−**c**). During cooling of **2a** from the isotropic liquid, a partial crystallization occurs around 95 °C. Reheating of the sample results in a complete crystallization at 66 °C followed by melting into the isotropic liquid at 138 °C, as observed in a previous thermal cycle. In contrast, **2b** exhibits more complex phase behavior with one endothermic and three exothermic events in the heating curve (Figure 11). The exothermic event at 7 °C and the two endothermic events at −13 and 92 °C belong to solid−solid phase transitions as evidenced by POM. At 114 °C a smectic mesophase is formed. This phase can be assigned on the basis of its optical defect textures: oily streak textures were observed by POM (Figure 13). At 149 °C **2b** melts into an isotropic liquid. Three exothermic peaks were observed during cooling, which were attributed to L_{iso} → SmA (144 °C), SmA → Cr″ (85 °C), and Cr″ → Cr′ (76 °C) transitions. **2c** exhibits a smectic A phase at 164 °C upon cooling the isotropic liquid. No crystallization occurs during further cooling, but at 56 °C upon reheating. The smectic A phase is then formed (126 °C) before the clearing point is reached at 167 °C. Within this group of azobenzene salts the clearing points increase with increasing chain length, and the compound with the longest alkyl chain (**2c**) has the largest mesophase temperature window. The thermal behavior of these three compounds differs significantly, reflected by the distinctly different crystals structures.

The compounds **3a**−**d** do not show any liquid crystalline behavior (Figure 12). Peaks in addition to the melting peaks can be attributed to solid−solid phase transitions (Table 1). No trend for the melting temperatures of these ILs can be recognized: **3a** and **3b** melt around 75 °C, melting of **3c** starts at 98 °C, and **3d** with an even longer alkyl chain melts at 86 °C. However, the salt with the longest alkyl chain (C16, **3e**) exhibits a smectic A phase in a very narrow temperature window (97−86 °C) when cooling the molten salt (Table 2). Such a mesophase formation was not observed upon heating the other compounds like **3d**. **3d** directly melts from the crystalline into the liquid phase (Figure 12). As **3c** and **3e** are isostructural, it seems to be valid to assume that the structures of all other compounds in this series are similar, too. This allows us to conclude that the length of the alkyl chain length essentially determines the ability to form a mesophase. With 16 carbon atoms the alkyl chain of **3e** is long

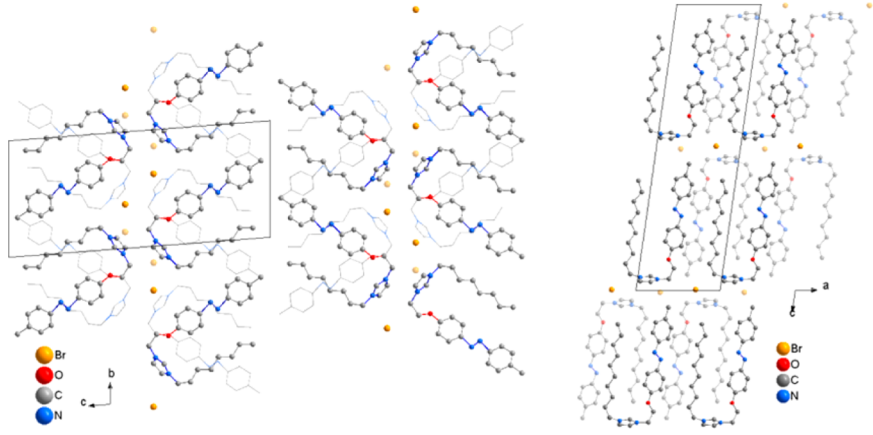

Figure 6. Crystal structure of **2a** (left), **2b** (right). For clarity the H atoms are omitted and some ions are displayed transparent.

DOI: 10.1021/acs.cgd.5b01024
Cryst. Growth Des. 2015, 15, 4701−4712

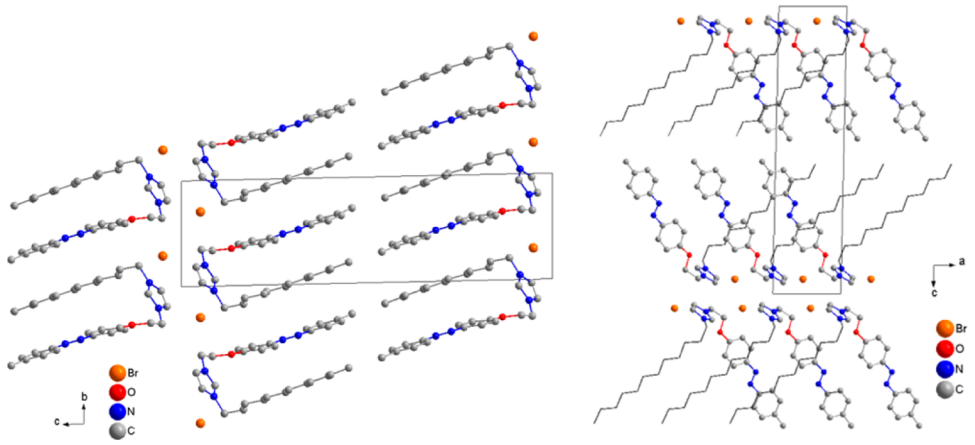

Figure 7. Crystal structure of **2c**.

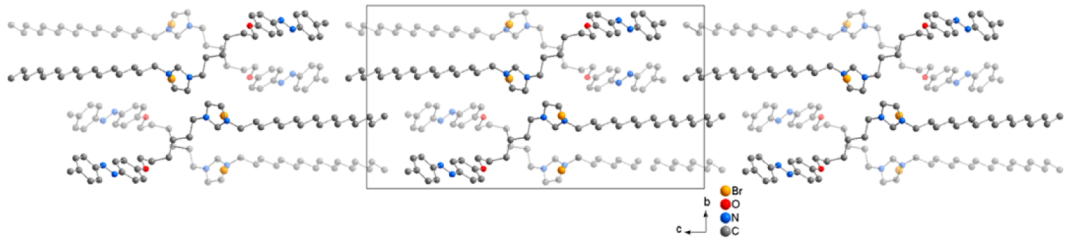

Figure 8. Crystal structure of **3e** viewed along the *a*-axis.

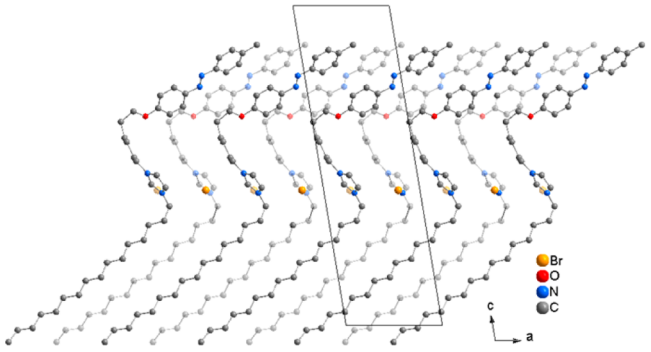

Figure 9. Crystal structure of **3e** viewed along the *b*-axis.

enough to separate the polar domains in the ion packing (compare Figure 8) and to allow the ions to form a smectic A phase before melting to the isotropic liquid. The identification of transition temperatures and the proof of mesophase formation were undertaken by POM. Figure 13 shows some representative POM textures for observed mesophases obtained by heating and cooling of the compounds.

Small Angle X-ray Scattering. To identify the mesophases of the symmetric compounds **1a**−**e** and to comprehend the molecular arrangement of the azobenzene salts temperature-dependent SAXS measurements were carried out. The layer distances, as calculated from Bragg's law, are listed in Table 3.

The distance of 14 Å observed from SAXS for **1a** can be identified as the layer spacing in the crystal structure. As compounds **1b** and **1c** show a similar layer distance the same molecular arrangement can be assumed. Upon further extension of the alkyl chain (C12 and C14) the crystal structure changes and a significantly larger layer distance was measured (Table 3). For that reason, an interdigitated rod-shaped structure is supposed for compounds **1d** and **1e** in the crystalline phase. The layer spacing increases when the mesophase is adopted, as commonly observed for smectic A phases (Figure 14).

Photochromic Properties. The UV−vis spectra **1b**, **2a**, and **3a** dissolved in methanol are shown in Figure 15. (UV−vis spectra of all 13 compounds can be found in the Supporting Information.) All compounds show similar absorption spectra with an absorption band maximum around 340 nm, a weaker absorption band around 230 nm, and a very weak band around 440 nm. The band at 340 nm can be assigned to the $\pi-\pi^*$ transition of the *trans* isomer and the one at 440 to the $n-\pi^*$ transition, as observed in similar compounds.[17,25] The $\pi-\pi^*$ band is clearly blue-shifted for the symmetrical azobenzene compounds (**1a**−**c**): 321 nm compared to 343 or 348 nm for the asymmetric azobenzene salts (**2a**−**c** and **3a**−**e**). This is due to the different substitution of the azobenzene moiety: alkyl for **1a**−**c** and alkoxy for compounds **2a**−**c** and **3a**−**e**. The red shift of 5 nm from 343 nm (**2a**) to 348 nm (**3a**) might be due to the electron-donating ability of the alkyl groups. The same shifts can be observed for the weaker absorption bands at 222, 236, and 239 nm, respectively. However, no shift for the $n-\pi^*$ band is found. For all compounds this weak band lies at 440 nm.

Azobenzene compounds undergo *cis*−*trans* isomerization when irradiated with the appropriate wavelength. After synthesis the compounds are mainly in the thermodynamically stable *trans* conformation which then can be switched to the *cis* conformation by irradiation with UV-light (Figure 16). When irradiating **1a** with UV-light (366 nm) a decrease in the strong $\pi-\pi^*$ absorption band (321 nm) and a simultaneous increase in the weak absorption band at 440 nm are observed (Figure 16). Additionally a new absorption band at 249 nm grows, while the weak band at 222 nm disappears. This change can be detected in transmission measurements on methanolic solutions as well as in reflectance measurements on the pure sample (Figure 16). It was not possible to observe the isomerization in the liquid crystalline

DOI: 10.1021/acs.cgd.5b01024
Cryst. Growth Des. 2015, 15, 4701−4712

Table 2. Transition Temperatures and Enthalpies Obtained from DSC Thermograms

		heating[a]			cooling[a]		
no.	formula	transition[b]	T [°C]	ΔH [kJ/mol]	T [°C]	ΔH [kJ/mol]	T_d[c] [°C]
1a	**Azo(-C1-Im-C6)$_2$**	Cr → L_{ISO}	212.6	60.3			277
1b	**Azo(-C1-Im-C8)$_2$**	Cr → L_{ISO}	242.1	59.5			238
1c	**Azo(-C1-Im-C10)$_2$**	Cr→?	144.2	9.5			253
		? →L_{ISO}	222.2	55.4			
1d	**Azo(-C1-Im-C12)$_2$**	Cr→SmA	151.9	2.1			262
		SmA→L_{ISO}	181.4	10.3			
1e	**Azo(-C1-Im-C14)$_2$**	Cr‘→Cr	75.8	10.6			266
		Cr→SmA	101.7	9.5			
		SmA →L_{ISO}	184.6	9.9			
2a	**C1-Azo−O−C2-Im-C8**	Cr‘→Cr	66.3	−20.2			272
		Cr→L_{iso}	137.6	29.9	94.4	−2.4	
2b	**C1-Azo−O−C2-Im-C10**	Cr′→Cr	−13.2	0.5			267
		Cr→Cr′	7.8	−2.1			
		Cr′→Cr″	92.3	8.4	75.8	−1.0	
		Cr″→SmA	114.4	22.9	85.2	−20.4	
		SmA →L_{ISO}	146.9	3.8	144.3	−4.3	
2c	**C1-Azo−O−C2-Im-C12**	SmA→Cr	56.1	−16.4			264
		Cr→SmA	126.5	18.3			
		SmA →L_{ISO}	167.0	2.7	164.2	−2.9	
3a	**C1-Azo−O−C6-Im-C8**	Cr→Cr′	24.2	−20.9			268
		Cr′→Cr	62.4	1.6			
		Cr′ →L_{ISO}	75.1	12.5			
3b	**C1-Azo−O−C6-Im-C10**	Cr′→Cr	20.9	−10.4			267
		Cr′ →L_{ISO}	74.7	40.4	25.1	−11.0	
3c	**C1-Azo−O−C6-Im-C12**	Cr′→Cr	92.9	40.8	45.1	−13.1	270
		Cr′ →L_{ISO}	98.0		77.4	−7.0	
3d	**C1-Azo−O−C6-Im-C14**	Cr′→Cr	24.7	2.2	23.8	−1.4	273
		Cr′ →L_{ISO}	85.8	28.3	79.3	−15.3	
3e	**C1-Azo−O−C6-Im-C16**	Cr →L_{ISO}	99.6	31.7			280
		S →Cr			84.6	−2.6	
		L_{ISO} → SmA			96.9	−31.6	

[a]Phase-transition temperatures (°C) and enthalpies (kJ/mol, in parentheses) are measured during heating and cooling at 5 K/min. [b]The phase transitions were identified by POM and SAXS measurements. [c]Thermal decomposition temperature.

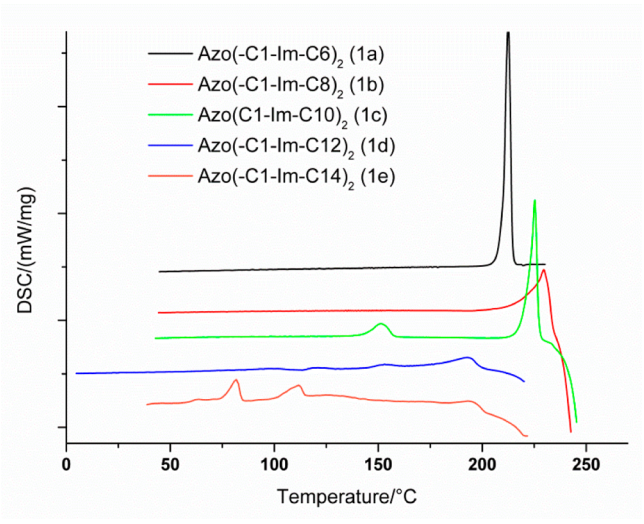

Figure 10. DSC heating traces of compounds **1a−e**.

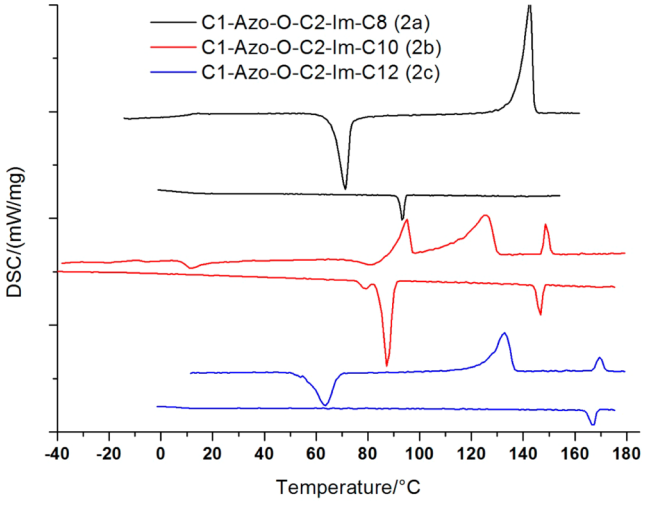

Figure 11. DSC heating traces of compounds **2a−c**.

phase, because the temperatures are too high and the thermal back reaction takes place, so that no *cis* form is accumulated.

This photoisomerization is reversible and can be monitored through the change in absorbance at a certain wavelength (Figure 17A). With these measurements the photoisomerization effective conversion constant k can be calculated for the *trans* to *cis* conversion and for the *cis* to *trans* isomerization (Table 3). The effective conversion constants of the two reactions cannot be compared directly, because the intensities of the absorbance and of the irradiation light are different for the two species. However,

DOI: 10.1021/acs.cgd.5b01024
Cryst. Growth Des. 2015, 15, 4701−4712

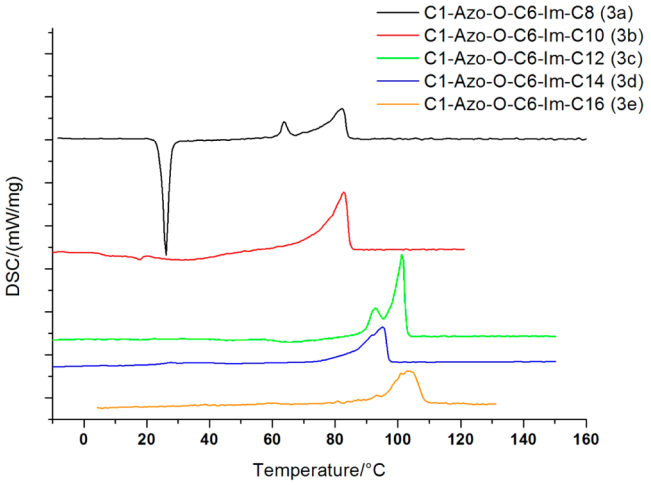

Figure 12. DSC heating traces of compounds **3a**–**e**.

a comparison within the series of synthesized compounds is possible. For the symmetric compounds **1a**–**e** a significant decrease in effective conversion constant with increasing chain length is observed for both conversions. The *trans*–*cis* isomerization is slowed down when the alkyl chains become longer. For the asymmetric compounds **2a**–**c** and **3a**–**e** with the azobenzene group at one end, no significant influence of the alkyl chain length on the isomerization rate was found. The influence of the solvent on the effective conversion constant was investigated for compound **2b** (Figure 17B). To this avail, effective conversion constants were determined for solutions of **2b** in solvents of different polarity (Table 3). The solvents can be ordered with decreasing effective conversion constant: MeOH > EtOH > PrOH > BuOH > THF. The isomerization is slowed down with decreasing polarity.

CONCLUSION

A set of 13 new azobenzene-based bromide salts were synthesized, and their thermal and photochromic properties were investigated. Two different systems based on imidazolium cations were studied: a monocation, featuring a *n*-alkylimidazolium group connected via an alkoxy chain (ethyl or hexyl) to a terminal azobenzene unit, and a symmetrical bication with a azobenzene group linking to two imidazolium rings which are substituted with alkyl chains. The alkyl chain length was systematically varied to see the influence on the thermal and photophysical behavior. All bicationic compounds decompose during the melting process. The salts with the longest alkyl chains (**1d** and **1e**) exhibit a liquid crystalline phase from 150/102 °C until 181/184 °C. The compounds with a terminal azobenzene group and a long alkoxy chain ($-OC_6H_{12}-$, **3a**–**3e**) qualify as ILs as they melt below 100 °C. In the solid state, when the

Table 3. Layer Spacing (*d*, Å) of Compounds 1a–e

no.	formula	25 °C	150 °C	180 °C
1a	**Azo(-C1-Im-C6)$_2$**	14		
1b	**Azo(-C1-Im-C8)$_2$**	13.4		
1c	**Azo(-C1-Im-C10)$_2$**	14.4		
1d	**Azo(-C1-Im-C12)$_2$**	38.6	39.7	
		19.2	19.7	
		12.7	13.1	
1e	**Azo(-C1-Im-C14)$_2$**	54.4	56.6	
		38.6	42.9	42.9
		19.2	21.5	
		12.8	14.1	14.2
		9.6	10.6	10.7

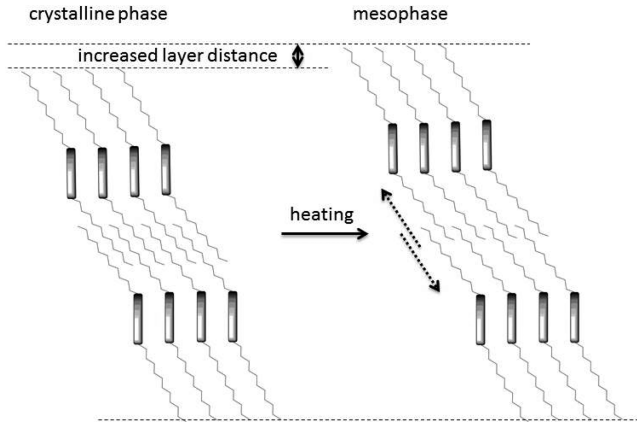

Figure 14. Schematic model of the molecular arrangement in the smectic A phase of compounds **1d** and **1e**.

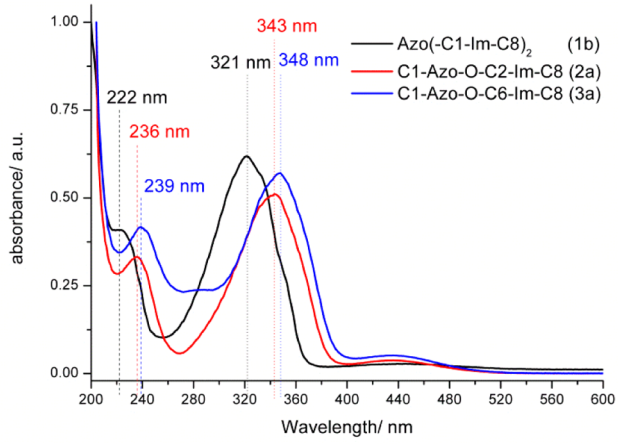

Figure 15. Normalized UV–vis spectra of compounds **1b**, **2a**, and **3a**.

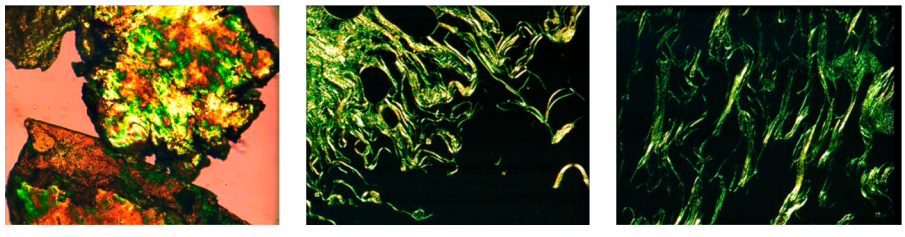

Figure 13. Representative textures as seen between crossed polarizers: (left) LC phase of **1b** at 137.6 °C, (middle) SmA phase of **2b** at 100.3 °C, (right) SmA phase of **3e** at 82.7 °C.

DOI: 10.1021/acs.cgd.5b01024
Cryst. Growth Des. 2015, 15, 4701–4712

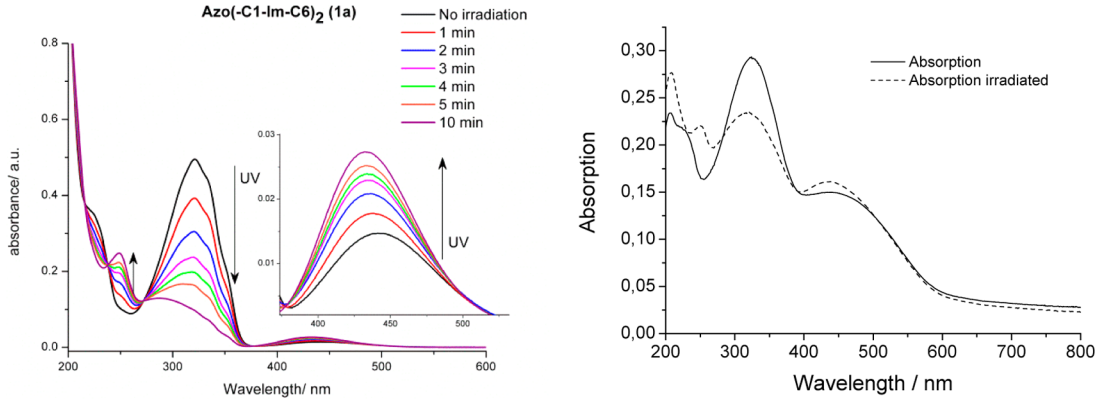

Figure 16. Left: change of the extinction coefficient of compound **1a** in methanol when irradiated with UV-light (366 nm); right: change of the absorption of a solid sample upon irradiation.

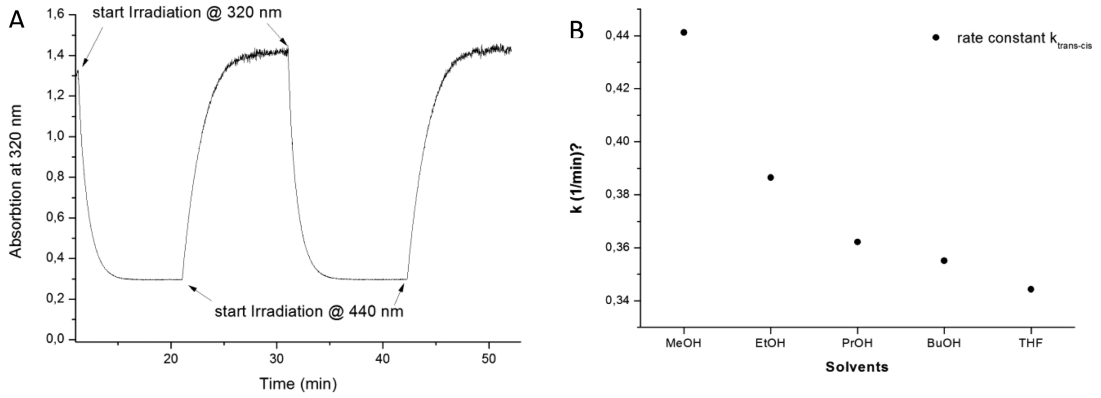

Figure 17. (A) Time evolution of absorbance of **1a** at 320 nm upon UV and visible light irradiation. (B) Effective conversion constant *k* of **2b** in dependency of the solvent.

Table 4. Calculated Effective Conversion Constants of All Compounds

compound	solvent	$k_{trans-cis}$ (1/min)	$k_{cis-trans}$ (1/min)
1a	MeOH	0.60978	0.47528
1b	MeOH	0.12996	0.10283
1c	MeOH	0.10718	0.08438
1d	MeOH	*a*	*a*
1e	MeOH	*a*	*a*
2a	MeOH	0.40176	0.1094
2b	MeOH	0.44124	0.11186
2c	MeOH	0.43997	0.11055
3a	MeOH	0.47929	0.11418
3b	MeOH	0.43037	0.12394
3c	MeOH	0.44149	0.1225
3d	MeOH	0.42897	0.12205
3e	MeOH	0.52874	0.12056
2b	EtOH	0.38644	0.09238
2b	PrOH	0.36214	0.10991
2b	BuOH	0.35508	0.09671
2b	THF	0.34428	0.07728

[a]Not measured.

connecting carbon chain is longer ($-OC_6H_{12}-$) an elongated rod-shape is adopted by the cation, in contrast to the cations with a short alkoxy-bridge ($-OC_2H_4-$), where the cations form a U-shape. For the U-shaped cations bearing an ($-OC_2H_4-$) bridge, the terminal alkyl chain influences the ion packing. The U-shaped cations either form a head-to-head tilted bilayer (**2a**), a head-to-tail single layer (**2b**), or head-to-head linear bilayer with an opened U (L) shape (**2c**). A smectic A phase is formed by the cations with a short alkoxy chain and a long alkyl chain (**2b** and **2c**) and by the cation with the longer alkoxy chain and the longest alkyl chain (**3e**). The synthesis affords all compounds in the thermodynamically stable *trans* conformation. By irradiation with UV-light (320−366 nm) they undergo a *trans*−*cis* isomerization which reverses under visible light (440 nm). The effective conversion constants of these reactions were calculated and show that the chain length has no influence on the photoisomerization of compound with terminal azobenzene units, but in the bicationic compounds the long alkyl chains hinder the isomerization process. The influence of the photoisomerization on the mesophase could not be investigated, because the liquid crystalline phases of these cations are formed at high temperatures (>100 °C), where the thermal reverse reaction is faster than the UV-induced *trans*−*cis* transformation. Thus, to develop photoswitchable ILCs the phase transition temperatures need to be further lowered.

■ ASSOCIATED CONTENT

Supporting Information

The Supporting Information is available free of charge on the ACS Publications website at DOI: 10.1021/acs.cgd.5b01024.

Crystal structure of compound **3c**, table of crystallographic and refinement details, normalized UV-Vis spectra (PDF)
Crystallographic information file for $C_{32}H_{44}Br_2N_6$ (CIF)
Crystallographic information file for $C_{26}H_{35}BrN_4O$ (CIF)

DOI: 10.1021/acs.cgd.5b01024
Cryst. Growth Des. 2015, 15, 4701−4712

Crystallographic information file for $C_{28}H_{39}BrN_4O$ (CIF)
Crystallographic information file for $C_{30}H_{43}BrN_4O$ (CIF)
Crystallographic information file $C_{34}H_{51}BrN_4O$ (CIF)
Crystallographic information file $C_{38}H_{59}BrN_4O$ (CIF)

AUTHOR INFORMATION

Corresponding Author

*E-mail: anja.mudring@ruhr-uni-bochum.de, mudring@iastate.edu. Tel: +49-234-32-27408, +1 515 5095616.

Notes

The authors declare no competing financial interest.

ACKNOWLEDGMENTS

This work was supported in part by the German Science Foundation DFG, Iowa State University, and the Critical Materials Institute, an Energy Innovation Hub funded by the U.S. Department of Energy, Office of Energy Efficiency and Renewable Energy, Advanced Manufacturing Office.

REFERENCES

(1) Wasserscheid, P.; Welton, T., Eds. *Ionic Liquids in Synthesis*; Wiley-VCH: Weinheim, Germany, 2003.
(2) Plechkova, N. V.; Seddon, K. R. *Chem. Soc. Rev.* **2008**, *37*, 123.
(3) Freemantle, M. *Chem. Eng. News* **1998**, *76*, 32−37.
(4) Welton, T. *Chem. Rev.* **1999**, *99* (8), 2071−2084.
(5) O'Reagan, B.; Grätzel, M. *Nature* **1991**, *353*, 737.
(6) Endres, F.; MacFarlane, D.; Abbott, A., Eds. *Electrodeposition from Ionic Liquids*; Wiley-VCH: Weinheim, Germany, 2008.
(7) Hough, W. L.; Smiglak, M.; Rodrıguez, H.; Swatloski, R. P.; Spear, S. K.; Daly, D. T.; Pernak, J.; Grisel, J. E.; Carliss, R. D.; Soutullo, M. D.; Davis, J. H., Jr.; Rogers, R. D. *New J. Chem.* **2007**, *31*, 1429−1436.
(8) Xu, F.; Matsumoto, K.; Hagiwara, R. *J. Phys. Chem. B* **2012**, *116*, 10106−10112.
(9) Kohler, F. T. U.; Morain, B.; Weiß, A.; Laurin, M.; Libuda, J.; Wagner, V.; Melcher, B. U.; Wang, X.; Wasserscheid, P.; Meyer, K. *ChemPhysChem* **2011**, *12*, 3539−3546.
(10) Sobota, M.; Wang, X.; Fekete, M.; Happel, M.; Meyer, K.; Wasserscheid, P.; Laurin, M.; Libuda, J. *ChemPhysChem* **2010**, *11*, 1632−1636.
(11) Lee, K. W.; Lee, C. K.; Lin, I. J. B. *Chem. Commun.* **1997**, 899.
(12) Bradley, A. E.; Hardacre, C.; Holbrey, J. D.; Johnston, S.; McMath, S. E. J.; Nieuwenhuyzen, M. *Chem. Mater.* **2002**, *14*, 629−635.
(13) Stappert, K.; Ünal, D.; Mallick, B.; Mudring, A.-V. *J. Mater. Chem. C* **2014**, *2*, 7976−7986.
(14) Li, X.; Bruce, D. W.; Shreeve, J. M. *J. Mater. Chem.* **2009**, *19*, 8232−8238.
(15) Zeng, Z.; Phillips, B. S.; Xiao, J.-C.; Shreeve, J. M. *Chem. Mater.* **2008**, *20*, 2719−2726.
(16) Yang, M.; Stappert, K.; Mudring, A.-V. *J. Mater. Chem. C* **2014**, *2*, 458−473.
(17) Bara, J. E.; Hatakeyama, E. S.; Wiesenauer, B. R.; Zeng, X.; Noble, R. D.; Gin, D. L. *Liq. Cryst.* **2010**, *37* (12), 1587−1599.
(18) Axenov, K. V.; Laschat, S. *Materials* **2011**, *4*, 206−259.
(19) Dobbs, W.; Douce, L.; Heinrich, B. *Beilstein J. Org. Chem.* **2009**, *5*, 62, DOI: 10.3762/bjoc.5.62.
(20) Kouwer, P. H. J.; Swager, T. M. *J. Am. Chem. Soc.* **2007**, *129*, 14042−14052.
(21) Kumar, S.; Gupta, S. K. *Tetrahedron Lett.* **2010**, *51*, 5459−5462.
(22) Zhang, Q.; Jiao, L.; Shan, C.; Hou, P.; Chen, B.; Xu, X.; Niu, L. *Liq. Cryst.* **2008**, *35*, 765−772.
(23) Alcalá, R.; Giménez, R.; Oriol, L.; Piñol, M.; Serrano, J. L.; Villacampa, B.; Viñuales, A. I. *Chem. Mater.* **2007**, *19*, 235−246.
(24) Forber, C. L.; Kelusky, E. C.; Bunce, N. J.; Zerner, M. C. *J. Am. Chem. Soc.* **1985**, *107*, 5884−5890.
(25) Qi Ya, Q.; Dong, X.-Z.; Chen, W.-Q.; Duan, X.-M. *Dyes Pigm.* **2008**, *79*, 159−165.
(26) Natansohn, A.; Rochon, P.; Gosselin, J.; Xie, S. *Macromolecules* **1992**, *25*, 2268−2273.
(27) Ikeda, T.; Tsutsumi, O. *Science* **1995**, *268*, 1873−1875.
(28) Kim, D. Y.; Tripathy, S. K.; Li, L.; Kumar, J. *Appl. Phys. Lett.* **1995**, *66*, 1166−1168.
(29) Kang, H. C.; Lee, B. M.; Yoon, J.; Yoon, M. *J. Colloid Interface Sci.* **2000**, *231*, 255−264.
(30) Xiao, S.; Lu, X.; Lu, Q.; Su, B. *Macromolecules* **2008**, *41*, 3884−3892.
(31) Zhang, Q.; Shan, C.; Wang, X.; Chen, L.; Niu, L.; Chen, B. *Liq. Cryst.* **2008**, *11*, 1299−1305.
(32) Yam, V. W. W.; Lee, J. K. W.; Ko, C. C.; Zhu, N. Y. *J. Am. Chem. Soc.* **2009**, *131*, 912.
(33) Zhang, S.; Liu, S.; Zhang, Q.; Deng, Y. *Chem. Commun.* **2011**, *47*, 6641−6643.
(34) SIR-92: Altomare, A.; Cascarano, G.; Giacovazzo, G.; Guagliardi, A. *J. Appl. Crystallogr.* **1993**, *26*, 343.
(35) Sheldrick, G. M. *SHELXL-97, Programs for Crystal Structure Analysis*; University of Göttingen: Germany, 1997.
(36) *X-RED, v. 1.22, Stoe Data Reduction Program (C)*; Stoe & Cie GmbH: Darmstadt, Germany, 2001.
(37) *X-Shape, v. 1.06, Crystal Optimisation for Numerical Absorption Correction (C)*; Stoe & Cie GmbH: Darmstadt, 1999.
(38) Brandenburg, K.; Putz, H. *DIAMOND, Program for Crystal and Molecular Structure Visualization*; Crystal Impact GbR: Bonn, Germany.

DOI: 10.1021/acs.cgd.5b01024
Cryst. Growth Des. 2015, 15, 4701−4712